Atmospheric
Chemistry
and Physics

Enhanced natural releases of mercury in response to the reduction in anthropogenic emissions during the COVID-19 lockdown by explainable machine learning

Xiaofei Qin[1], Shengqian Zhou[1], Hao Li[1], Guochen Wang[1], Cheng Chen[1], Chengfeng Liu[1], Xiaohao Wang[2], Juntao Huo[2], Yanfen Lin[2], Jia Chen[2], Qingyan Fu[2], Yusen Duan[2], Kan Huang[1,3,4], and Congrui Deng[1]

[1]Center for Atmospheric Chemistry Study, Shanghai Key Laboratory of Atmospheric Particle Pollution and Prevention (LAP3), National Observations and Research Station for Wetland Ecosystems of the Yangtze Estuary, Department of Environmental Science and Engineering, Fudan University, Shanghai 200433, China
[2]State Ecologic Environmental Scientific Observation and Research Station for Dianshan Lake, Shanghai Environmental Monitoring Center, Shanghai 200030, China
[3]Institute of Eco-Chongming (IEC), Shanghai 202162, China
[4]IRDR ICoE on Risk Interconnectivity and Governance on Weather/Climate Extremes Impact and Public Health, Fudan University, Shanghai 200433, China

Correspondence: Kan Huang (huangkan@fudan.edu.cn) and Congrui Deng (congruideng@fudan.edu.cn)

Abstract. The wide spread of the coronavirus (COVID-19) has significantly impacted the global human activities. Compared to numerous studies on conventional air pollutants, atmospheric mercury that has matched sources from both anthropogenic and natural emissions is rarely investigated. At a regional site in eastern China, an intensive measurement was performed, showing obvious decreases in gaseous elemental mercury (GEM) during the COVID-19 lockdown, while it was not as significant as most of the other measured air pollutants. Before the lockdown, when anthropogenic emissions dominated, GEM showed no correlation with temperature and negative correlations with wind speed and the height of the boundary layer. In contrast, GEM showed significant correlation with temperature, while the relationship between GEM and the wind speed/boundary layer disappeared during the lockdown, suggesting the enhanced natural emissions of mercury. By applying a machine learning model and the SHAP (SHapley Additive exPlanations) approach, it was found that the mercury pollution episodes before the lockdown were driven by anthropogenic sources, while they were mainly driven by natural sources during and after the lockdown. Source apportionment results showed that the absolute contribution of natural surface emissions to GEM unexpectedly increased (44 %) during the lockdown. Throughout the whole study period, a significant negative correlation was observed between the absolute contribution of natural and anthropogenic sources to GEM. We conclude that the natural release of mercury could be stimulated to compensate for the significantly reduced anthropogenic GEM via the surface–air exchange in the balance of mercury.

1 Introduction

Mercury pollution has received widespread attention due to its long-range transport, bioaccumulation, and neurotoxicity (Giang and Selin, 2016; Horowitz et al., 2017; Driscoll et al., 2013). The atmosphere is the key to the distribution of mercury on a global scale because gaseous elemental mercury (the predominant form of mercury in the atmosphere at >90 %) has relatively high stability and long residence time and can be transported through the atmosphere over long distances (Xu et al., 2017; Mao et al., 2016). Mercury in the atmosphere derives from both anthropogenic emissions and natural processes. The main anthropogenic sources of atmospheric mercury include coal combustion, nonferrous smelters, cement production, waste incineration, and mining (Wu et al., 2018, 2016). The amount of mercury in the atmosphere directly emitted by anthropogenic activities accounted for about 30 % of the global mercury emissions (Streets et al., 2019; Steenhuisen and Wilson, 2019), and China is the country with the largest anthropogenic atmospheric mercury emissions in the world (Liu et al., 2019). The natural sources of mercury in the atmosphere are mainly from the exchange processes between natural surfaces (e.g., soil, vegetation, and water) and the atmosphere (Outridge et al., 2018; Pirrone et al., 2010). Unlike anthropogenic emissions, natural releases of mercury are passive emissions and are susceptible to various environmental factors, such as meteorological parameters (e.g., solar radiation, temperature, and atmospheric turbulence), surface properties (e.g., soil/water mercury content, organic matter, and microbial activity), and ambient air characteristics (e.g., Hg^0 concentration and O_3 concentration in the atmosphere; Zhu et al., 2016). Previous studies have focused on the effects of various meteorological factors and different medium properties on natural surface releases of mercury. The soil Hg^0 flux and solar radiation showed a high positive correlation, which was generally considered to be due to the high solar radiation tending to promote the reduction of Hg^{II} to Hg^0 (Carpi and Lindberg, 1997; Poissant et al., 2004; Bahlmann et al., 2006). High wind speed was conductive to the release of mercury from seawater (Wanninkhof, 2014). The terrestrial vegetation acted as a global mercury pump (Jiskra et al., 2018), and deforestation would increase forest floor radiation and temperature, thereby increasing Hg^0 emissions (Carpi et al., 2014; Mazur et al., 2014). However, few studies have investigated the impact of changes in ambient gaseous elemental mercury (GEM) concentration in response to the natural surface emissions of Hg^0. In the context of the global annual decrease in the Hg^0 concentration (Zhang et al., 2016b), it is particularly urgent and important to conduct such research.

China has taken many stringent and ambitious control measures since 2013 to tackle its severe air pollution, such as imposing ultra-low-emission standards on coal-fired power plants and phasing out small- and high-emission factories (Zheng et al., 2018). These pollution control measures co-

benefited the significant reduction in anthropogenic mercury emissions (Wen et al., 2020; Liu et al., 2018). The anthropogenic atmospheric mercury emissions of China fell by 22 % from 2013 to 2017 (Liu et al., 2019), and correspondingly, decreasing trends in the annual mean atmospheric mercury concentration were observed both at Chinese urban and remote sites (Qin et al., 2020; Tang et al., 2018; Yin et al., 2018). In this regard, this change could be likely to affect the surface–air exchange balance of mercury. In early 2020, China's lockdown measures to control the spread of the 2019 novel coronavirus (COVID-19) resulted in a significant reduction in the emissions of primary air pollutants (Chang et al., 2020). One study in the Beijing–Tianjin–Hebei region showed that the anthropogenic emissions of atmospheric mercury reduced by about 22 % during the lockdown compared to that before the lockdown (Wu et al., 2021). Therefore, the COVID-19 lockdown provided a natural experiment to explore how the natural surface emissions of mercury would respond to the dramatic reduction in anthropogenic mercury emissions. Traditionally, chemical transport models were the most widely used tools for disentangling the contributions from meteorology and various emission sources, while the performance of these models relied heavily on the availability of updated emission inventories with high accuracy (Selin et al., 2007; Holmes et al., 2010; Huang and Zhang, 2021). Therefore, applying traditional models to reproduce and explain some special events and processes of atmospheric mercury could be limited by certain uncertainties. Recently, data-driven methods such as machine learning have been widely used in atmospheric science research (Grange et al., 2018; Vu et al., 2019; Qi et al., 2019). The model performance of machine learning in predicting atmospheric pollutants (such as $PM_{2.5}$) was generally better than traditional chemical transport models (Hou et al., 2022; Yang et al., 2021); however, these results were less robust in terms of interpretability due to the "black box" nature of the machine learning model. With the development of data analysis methods, tools that can unlock the mystery of machine learning have been emerging, such as the SHapley Additive exPlanations (SHAP) approach (Stirnberg et al., 2021). Therefore, combined with new interpretation methods, machine learning can be a promising alternative to study the behavior of pollutants in the atmosphere. However, few studies have applied machine learning to the study of atmospheric mercury.

Many receptor-based models have been used to determine the sources and processes of air pollutants, among which the positive matrix factorization (PMF) is a commonly used method (Yu et al., 2019; Sun et al., 2016; Chang et al., 2018). The PMF method provides quantitative source profiles and source contributions, and the obtained source profiles can aid factor interpretation (Belis et al., 2013). Another strength of PMF is that the measurement uncertainty is included in the PMF model, which ensures that species with large uncertainties have less impact on the model results (Hopke, 2016). Many previous studies have applied the PMF method to the

source apportionment of atmospheric mercury. One study in Canada compared the PMF model performance of atmospheric mercury in different years and found that the source profiles and source contributions of GEM in 2009 and 2010 were in good agreement (Xu et al., 2017). By using the PMF model, the research on the western coast of Ireland found that baseline and combustion processes were the controlling sources of atmospheric mercury (Custodio et al., 2020). The study in the Yangtze River Delta in eastern China suggested that the contribution of natural sources to GEM had gradually exceeded that of anthropogenic sources from 2015 to 2018 by using the PMF method (Qin et al., 2020). This indicated that it is feasible to use the PMF model to identify the sources of GEM in the atmosphere.

In this study, we first compared the concentration of GEM and its relationship with environmental factors before, during, and after the COVID-19 lockdown. Observational evidence on the changes in anthropogenic and natural sources of GEM was revealed. Then the drivers of the GEM variation throughout the study period were explored by using the machine learning model and explained by a game theoretic approach. Finally, we applied a receptor model to quantify the contribution of anthropogenic and natural sources to GEM and unveiled the response of natural releases of mercury to the reduction in anthropogenic mercury emissions.

2 Materials and methods

2.1 Site and instrumentation

Field measurements were conducted at the Dianshan Lake (DSL) site ($31.096°$ N, $120.988°$ E; 14 m a.g.l. – meters above ground level) at the junction of the Shanghai, Zhejiang, and Jiangsu provinces of the Yangtze River Delta (YRD) region of China (Fig. S1 in the Supplement). It represents a rural setting and the regional-scale air pollution characteristics of the YRD region. A detailed description of the site can be found in our previous works (Qin et al., 2019, 2020).

Ambient GEM concentration was measured by an automated mercury vapor analyzer (Tekran 2537B/1130/1135 system; Tekran Instruments Corporation, Canada) at a 5 min time resolution. More details on this instrument can be found elsewhere (Qin et al., 2019). Water-soluble ions in $PM_{2.5}$ (SO_4^{2-}, NO_3^-, NH_4^+, Cl^-, Na^+, K^+, Mg^{2+}, and Ca^{2+}) and water-soluble gases (NH_3 and SO_2) were continuously measured by the Monitor for AeRosols and Gases in ambient Air (MARGA) at a flow rate of $16.7\,L\,min^{-1}$, with a time resolution of 1 h (Wang et al., 2022b; Xu et al., 2020). Heavy metals in $PM_{2.5}$ (Pb, Fe, Ba, Cr, Se, Cd, Ag, Ca, Mn, Cu, As, Ni, Zn, and V) were determined hourly by a multimetal monitor (Xact^{TM} 625; Cooper Environmental Services, LLC, USA; Wang et al., 2022a). Black carbon in $PM_{2.5}$ was continuously measured by a multi-wavelength Aethalometer (AE33, Magee Scientific, USA; Li et al., 2021). Organic car-

bon (OC) and elemental carbon (EC) in $PM_{2.5}$ were measured by an in situ semi-continuous organic carbon and elemental carbon aerosol analyzer (RT-3195; Sunset Laboratory Inc., Beaverton, Oregon, USA; Xu et al., 2018). SO_2, CO, O_3, and $PM_{2.5}$ were determined by Thermo Scientific models 43i, 48i-TLE, 49i, and 1405-F, respectively. Meteorological parameters, including air temperature, relative humidity, wind speed, and wind direction, were collected by using a series of Vaisala weather sensors (WXT530 Weather Transmitter Series; Vaisala, Vantaa, Finland) with a time resolution of 10 min.

The air pollutants, including CO, NO_2, and $PM_{2.5}$ at other ground monitoring stations in the YRD region were obtained from the public database of the China National Environmental Monitoring Center.

The data of the planetary boundary layer (PBL) height were obtained from the U.S. National Oceanic and Atmospheric Administration (https://www.ready.noaa.gov/archives.php, last access: 31 August 2022). The 3 d air mass backward trajectories were calculated by applying the Hybrid Single-Particle Lagrangian Integrated Trajectory (HYSPLIT) model (https://www.ready.noaa.gov/HYSPLIT.php, last access: 31 August 2022), and MeteoInfo software was used to perform cluster analysis of backward trajectories.

2.2 Machine learning model

The artificial neural network (ANN) model was used to simulate the GEM concentration at the DSL site during the study period. An artificial neural network is a mathematical model based on the basic principles of neural networks in biology. The network structure consists of the input layer, hidden layer, and output layer of neurons. The process of obtaining an ANN model is that the neurons of input layer pass through each hidden layer and then reach the output layer. If the expected results are not obtained in the output layer, then the errors are propagated back, and the neuron weights of each hidden layer are iteratively updated to minimize them. In this study, the long-term observational air pollutants (SO_2, CO, O_3, NO_2, and $PM_{2.5}$) and meteorological data (air temperature, relative humidity, and wind speed) in Shanghai from 1 March 2015 to 28 February 2019 were chosen as input variables for training. These variables were directly or indirectly related to the emissions (both anthropogenic and natural sources), transport, and removal processes of GEM. For example, the main sources of SO_2, CO, and NO_2 were fossil fuel combustions, which were also the largest anthropogenic sources of GEM (Zhang et al., 2016a; Streets et al., 2011). The natural sources of GEM were mainly from the release of land and sea surfaces, which were closely related to temperature, relative humidity, and wind speed (Wang et al., 2014; Moore and Carpi, 2005).

The detailed training and validation of this model can be found in our previous study (Qin et al., 2022). We have estab-

lished an ANN model through training the long-term observational data of GEM and other auxiliary environmental parameters at DSL. The long-term observational GEM (hourly data from 1 March 2015 to 28 February 2019; $n = 17\,532$) in Shanghai was the target variable for training, and the corresponding air pollutants (SO_2, CO, O_3, NO_2, and $PM_{2.5}$) and meteorological data (air temperature, relative humidity, and wind speed) were chosen as input variables for training. The data sets were randomly divided into three parts, i.e., 70 % for training, 15 % for validation, and 15 % for testing. We chose the neural network containing a hidden layer with 20 nodes, and the training algorithm was the Levenberg–Marquardt. The performance of the model was evaluated with the mean square error (MSE) and correlation coefficient (R^2 value). To verify the accuracy of the trained neural network model, we compared the observed (not included in the training data set) and simulated GEM concentrations of DSL from 1 January to 26 February 2020 and found that they exhibited a reasonably good correlation with the correlation coefficient (R^2) of 0.67. To test the applicability of the model on the regional scale, we compared the observed and simulated GEM concentrations in Suzhou, Ningbo, Nanjing, and Hefei (Fig. S2). In Nanjing and Suzhou, the observed and simulated daily GEM were consistent, with R^2 values of 0.52 and 0.71, respectively. In Ningbo, the observed and simulated GEM in summer and winter were also consistent, with R^2 values of 0.64 and 0.65, respectively. A low bias was derived between the observed and simulated seasonal GEM in Hefei. This suggested that it was feasible to use the trained ANN model to simulate the GEM concentrations in Shanghai and even the Yangtze River Delta region.

2.3 SHapley Additive exPlanations (SHAP) approach

The SHAP approach was applied in this study to explain the ANN model simulation results. This approach constructs a distribution scheme based on the coalitional game theory that comprehensively considers the requirements of the conflicting parties, so as to ensure the fairness of the distribution (Lundberg et al., 2018, 2020; Hou et al., 2022). In the game theory, the Shapley value of a player represents the average contribution of the player in a cooperative game, which is a fair distribution of the total gain generated by individual players (Lundberg and Lee, 2017). In the context of machine learning prediction, the Shapley value of a feature at a query point represents the contribution of that feature to the prediction (response for regression or score of each class for classification) at a particular query point (Aas et al., 2021). The Shapley value corresponds to the deviation between the prediction for the query point and the average prediction caused by the feature, and the sum of the Shapley values for all features for specific query point corresponds to the total deviation of the prediction from the average (Kumar et al., 2020). The Shapley value of the ith feature for the query point x is defined by the value function v as follows:

$$\varphi_i(v_x) = \frac{1}{N}\sum_{S\subseteq\omega\setminus\{i\}} \frac{\frac{v_x(S\cup\{i\}) - v_x(S)}{(N-1)!}}{|S|!(N-|S|-1)!}, \tag{1}$$

where N is the number of all features, ω is the set of all features, $|S|$ is the cardinality of the set S or the number of elements in the set S, and v_x is the value function of the features in a set S for the query point x. The value of the function indicates the expected contribution of the features in S to the prediction for the query point x.

## 2.4 Positive matrix factorization (PMF)

The PMF model has proven to be a useful tool for obtaining source profiles and quantifying source contributions of complex air pollution (Gibson et al., 2015). The basic principle of PMF is that the concentration of the sample is determined by the source profiles with different contributions, which can be described as follows:

$$X_{ij} = \sum_{k=1}^{P} g_{ik}f_{kj} + e_{ij}, \tag{2}$$

where X_{ij} represents the concentration of the jth species in the ith sample, g_{ik} is the contribution of the kth factor in the ith sample, f_{kj} provides the information about the mass fraction of the jth species in the kth factor, e_{ij} is the residual for specific measurement, and P represents the number of factors. The number of factors being from three to eight was explored, with the optimal solutions determined by the slope of the Q value versus the number of factors. The Q value is the sum of the square of the difference between the measured and modeled concentrations weighted by the concentration uncertainties and needs to be minimized before the PMF modeled determines the optimal nonnegative factor profiles and contributions (Cheng et al., 2015).

$$Q = \sum_{i=1}^{n}\sum_{j=1}^{m}\left(\frac{X_{ij} - \sum_{k=1}^{p}A_{ik}F_{kj}}{S_{ij}}\right)^2,$$

where X_{ij} represents the concentration of the jth contamination in the ith sample, m is the total number of the pollutants, and n is the total number of samples. A_{ik} represents the contribution of the kth factor on the ith sample, and F_{kj} represents the mass fraction of the j pollutant in the kth factor. S_{ij} is the uncertainty in the jth pollutant on the ith factor, and P is the number of factors. For each run in this study, the stability and reliability of the outputs were assessed by referring to the Q value, residual analysis, and correlation coefficients between observed and predicted concentrations. Finally, we found that a six-factor solution showed the most stable results and gave the most reasonable interpretation. A detailed description can be seen in previous studies (Qin et al., 2020, 2019).
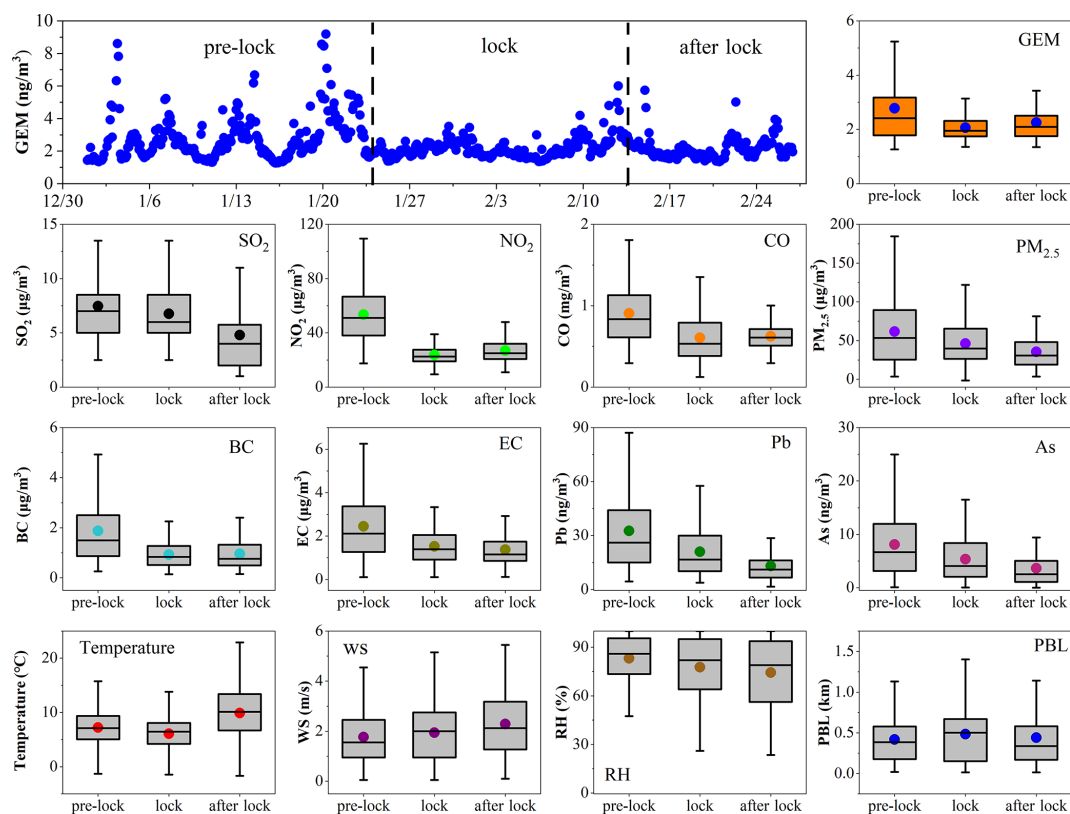
Figure 1. Hourly variations in GEM concentrations from 1 January to 26 February 2020. Box plots of GEM, SO_2, NO_2, CO, $PM_{2.5}$, BC, EC, Pb, As, and meteorological parameters (temperature, wind speed, relative humidity, and planetary boundary layer height) before, during, and after the lockdown are also shown.

3 Results and discussion

3.1 Changes in GEM concentrations during the lockdown

Figure 1 shows the time series of hourly GEM concentrations during 1 January to 26 February 2020. Three periods were defined, i.e., 1 to 23 January before the lockdown, 24 January to 14 February during the lockdown, and 15 to 26 February after the lockdown. Before the lockdown, hourly GEM showed strong fluctuations, with frequent extreme concentrations higher than 5 ng m^{-3}. In contrast, the diurnal variation in GEM was significantly weakened, with hourly concentrations all lower than 4 ng m^{-3} during the lockdown. After the lockdown, GEM concentration was slightly higher than that of during the lockdown. On average, GEM declined sharply from 2.78 ng m^{-3} before the lockdown to 2.06 ng m^{-3} during the lockdown and then rose slightly to 2.26 ng m^{-3} after the lockdown. Figure 1 also shows that typical gaseous pollutants, such as sulfur dioxide (SO_2), nitrogen dioxide (NO_2), and carbon monoxide (CO), behaved similarly to GEM, in addition to the $PM_{2.5}$ and its components such as black carbon (BC), elemental carbon (EC), lead (Pb), and arsenic (As). This temporal pattern was expected, as the nationwide reduction in automotive mobility and energy consumption

due to the COVID-19 lockdown would certainly have lead to drops in primary pollutants emissions. As shown in Fig. S3, the levels of CO, NO_2, and $PM_{2.5}$ in the Yangtze River Delta (YRD) declined sharply during the lockdown by 26 %, 61 %, and 27 %, respectively, which was consistent with emissions estimates based on up-to-date activity levels in eastern China (Huang et al., 2021). For anthropogenic Hg emissions, one study in the Beijing–Tianjin–Hebei region estimated a decline of approximately 22 % during the lockdown, which was mainly due to the reduction in cement clinker production, coal-fired power plants, and residential coal combustion (Wu et al., 2021). We compared the meteorological factors (including air temperature, wind speed, relative humidity, and planetary boundary layer height) before, during, and after the lockdown (Table S1). No significant changes in the meteorological factors were observed before and during the lockdown. In addition, the 3 d backward trajectory cluster analysis indicated that the transport patterns differed little between these two periods (Fig. S4). This suggested that the significant decline in GEM concentrations during the lockdown was mainly due to the reduced mercury emissions, rather than changes in synoptic conditions.
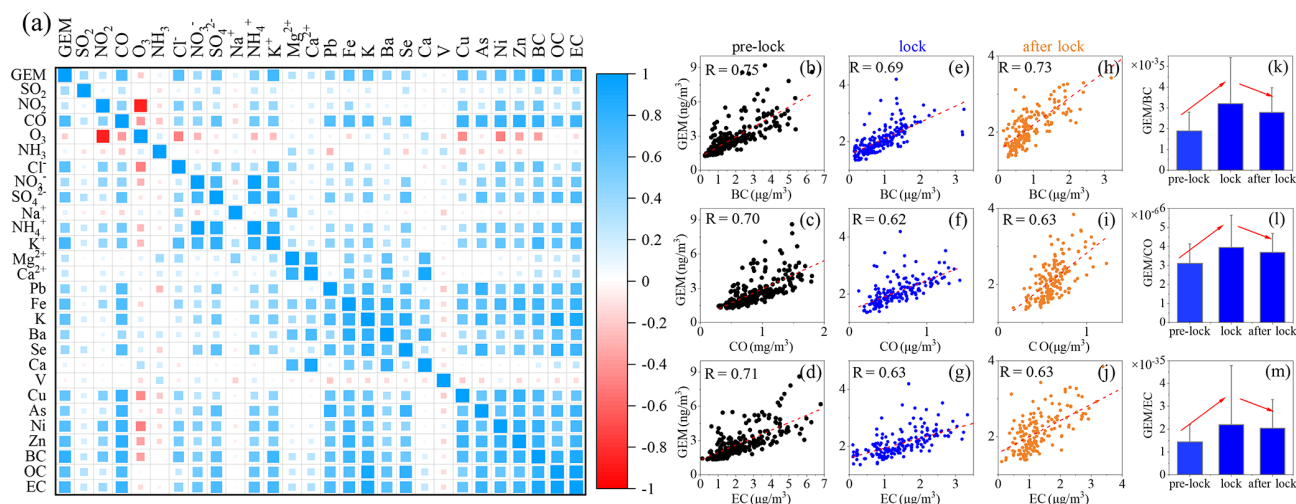
Figure 2. (a) Correlation coefficient matrix among GEM and $PM_{2.5}$ components and gaseous pollutants during the whole study period. Relationship between GEM and BC, CO, and EC **(b–d)** before, **(e–g)** during, and **(h–j)** after the lockdown. **(k–m)** The change in GEM/BC, GEM/CO, and GEM/EC ratios before, during, and after the lockdown.

3.2 Observational evidences of enhanced effects of natural sources on GEM

Table S2 further shows that the reduction rates of gaseous pollutants SO_2, NO_2, NO, and CO during the lockdown were 9 %, 56 %, 64 %, and 33 %, respectively, compared to those before the lockdown, while O_3 showed an almost 1-fold increase due to the strongly depressed titration effect from substantial reduced NO_x emissions during the lockdown (Huang et al., 2021; Yang et al., 2021). As for the primary trace elements such as Pb, Fe, Cr, Se, Ca, Mn, As, Ni, and Zn, their reduction rates ranged from 34 % to 73 %. As for the main chemical components in $PM_{2.5}$, NO_3^-, NH_4^+, and BC were strongly reduced by 58 %, 45 %, and 51 %, while SO_4^{2-} and OC were less reduced by 20 % and 16 %, respectively. Except for SO_2, SO_4^{2-}, and OC, GEM presented a lower reduction rate than the other air pollutants, probably indicating the discrepancy in key sources for different air pollutants. In order to probe the dynamic variation in GEM sources across the observational period, we first investigated the correlations among GEM and main components of $PM_{2.5}$ and gaseous pollutants (Fig. 2a). GEM was found to be significantly correlated with the primary air pollutants such as CO, K^+, BC, and EC, with the correlation coefficients (R) above 0.7. This suggested that the main anthropogenic sources of GEM might be coal combustion and biomass burning in Shanghai, which was consistent with the previous studies in the Yangtze River Delta (Qin et al., 2019; Tang et al., 2018).

BC, EC, and CO are mainly from fossil fuels combustion and biomass burning and can be used as indicators of the main anthropogenic sources of GEM. In order to explore the changes in the sources of GEM, we further investigated the relationship between GEM and BC/EC/CO before, during, and after the lockdown. As shown in Fig. 2, R be-

tween GEM and BC, GEM and CO, and GEM and EC during and after the lockdown were lower than that before the lockdown, suggesting the influence of anthropogenic sources on GEM was weakened during the lockdown. Different from BC, CO, and EC, which are overwhelmingly derived from anthropogenic sources, natural sources such as surface emission and ocean release also contribute significantly to GEM (Obrist et al., 2018). Hence, the ratio of GEM/BC, GEM/CO, and GEM/EC can be simply applied as indicators to reveal the relative importance of anthropogenic versus natural sources. A higher GEM/BC, GEM/CO, and GEM/EC ratio indicated the greater importance of natural sources, and vice versa. As shown in Fig. 2k–m, the GEM/BC ratio significantly increased from 1.9×10^{-3} before the lockdown to 3.2×10^{-3} during the lockdown, the GEM/CO ratio significantly increased from 3.1×10^{-6} to 4.0×10^{-6}, and the GEM/EC ratio significantly increased from 1.4×10^{-3} to 2.2×10^{-3}. The GEM/CO ratio has been used to analyze the sources of GEM in many studies. In this study, the GEM/CO ratio during the lockdown period was 4.0×10^{-6}, which was significantly higher than the anthropogenic GEM/CO emission ratio in mainland China, South Asia, and the Southeast Asian peninsula, whose values were 2.7, 2.6, and 1.5×10^{-6}, respectively (Fu et al., 2015). These values were also higher than the GEM/CO ratio observed in Nanjing (3.1×10^{-6}) and Beijing (1.5×10^{-6}) in winter (Zhang et al., 2013; Zhu et al., 2012). This corroborated that the impact of natural sources on GEM could be more outstanding during the lockdown than before and after the lockdown.

Previous studies have demonstrated the strong dependence of natural surface emissions on meteorological factors such as temperature, wind speed, and relative humidity (Pannu et al., 2014; Lindberg et al., 2007; Gustin et al., 2005). We com-
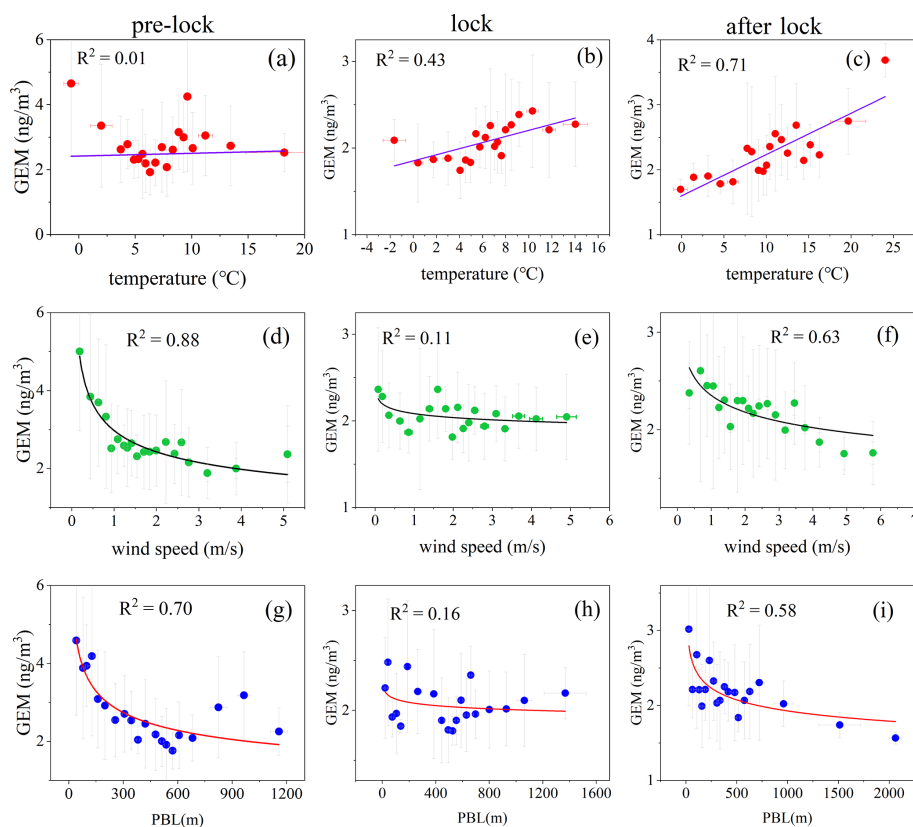
Figure 3. Relationship between GEM concentration and **(a–c)** temperature, **(d–f)** wind speed, and **(g–i)** PBL height before, during, and after the lockdown.

pared the relationship between GEM and meteorological parameters before, during, and after the lockdown to investigate the changes in natural sources of mercury. As shown in Fig. 3a–c, there was no clear correlation between GEM and temperature before the lockdown, while moderately high correlations during and after the lockdown emerged with the correlation coefficients (R^2) of 0.43 and 0.71, respectively. This might indicate the enhanced role of natural sources on GEM concentrations due to the lockdown control measures. For wind speed (Fig. 3d–f), strongly negative correlations were observed with GEM before and after the lockdown but not during the lockdown. On the one hand, the high wind speed was beneficial to the diffusion of air pollutants in the atmosphere, which explained the negative correlation between GEM and wind speed. On the other hand, the high wind speed promoted the natural surface release of mercury, partially canceling out the diffusion effect of the wind speed, which induced the ambiguous relationship between GEM and wind speed during the lockdown. The relationship between GEM and PBL height was similar to that of wind speed, showing strongly negative correlations before and after the lockdown while having weak correlations during the lockdown (Fig. 3g–i). The increase in PBL height was beneficial to the diffusion of GEM. While the increase in PBL

height usually occurred in the daytime when temperature was high, which was conducive to the natural surface release of mercury. Therefore, ambient GEM did not decrease significantly with the increase in PBL height during the lockdown.

Overall, all the observational evidence possibly suggested that the role of natural emissions on GEM was more manifested due to the lockdown. However, all the results were based on qualitative data analysis. In the following sections, the machine learning and source apportionment methods will be applied to quantify the contribution of anthropogenic and natural sources to GEM during the three defined periods.

3.3 Understanding the drivers of GEM variation by explainable machine learning

We further conducted machine learning simulations using the trained artificial neural network (ANN), which has already been established by training the long-term (2015–2019) observational data of GEM and other necessary environmental parameters (including SO_2, NO_2, CO, O_3, $PM_{2.5}$, temperature, relative humidity, and wind speed) at the Dianshan Lake site (Qin et al., 2022). Figure 4a–b show the comparison of ANN simulated and observed GEM concentrations during the whole study period and found that their correlation coefficient is acceptable ($R^2 = 0.67$). As shown in Fig. S5,

we examined the performance of the ANN model before, during, and after the lockdown. The correlations between ANN simulated and observed GEM concentrations were also acceptable, with correlation coefficients of 0.67, 0.59, and 0.63, respectively. Then we applied the SHapley Additive exPlanations (SHAP) approach to uncover the mystery of the machine learning "black box" model (see the methods in Sect. 2.3). This approach has the potential to quantify the global and local impacts of input features on model predictions (Lundberg and Lee, 2017), which has been used in various fields (Mangalathu et al., 2020; Hou et al., 2022; Lundberg et al., 2018; Zhong et al., 2021; Wang et al., 2021).

We calculated the SHAP value of each feature to represent the global importance of the feature, which can be used to indicate the general impact of various features across all samples. As shown in Fig. 4c, by comparing the average absolute SHAP values, $PM_{2.5}$ ranked as the most important feature, which changed the simulated GEM concentrations by $0.30 \pm 0.20 \, \mathrm{ng \, m^{-3}}$, followed by CO and temperature with the SHAP values of 0.16 ± 0.25 and $0.14 \pm 0.09 \, \mathrm{ng \, m^{-3}}$, respectively. The average values of the remaining factors were less than $0.1 \, \mathrm{ng \, m^{-3}}$. We further investigated the relationship between the SHAP value of each feature and its concentration. As shown in Fig. 4d–f, with the increase in $PM_{2.5}$, CO, and SO_2 concentrations, their corresponding SHAP values increased accordingly. Previous studies have shown that GEM, $PM_{2.5}$, CO, and SO_2 shared common anthropogenic sources, such as the combustion of fossil fuels and biomass (Chong et al., 2019; Fu et al., 2015), thus interpreting the positive effect of various anthropogenic emission sources on GEM. A similar relationship was also found for temperature and relative humidity with their corresponding SHAP values (Fig. 4g–h). Since temperature and relative humidity are important factors affecting the natural release of GEM from natural surfaces (Pannu et al., 2014; Wang et al., 2016), the positive influence of natural surface emissions on GEM was expected. In contrast, the SHAP value of wind speed negatively correlated with the magnitude of wind speed (Fig. 4i), thus indicating the diffusion/accumulation effect of wind speed on GEM. The SHAP values of NO_2 and O_3 did not show obvious correlations with their concentrations (Fig. 4j–k). One of the main sources of NO_2 was vehicle emissions, which contributed little to GEM. As for O_3, its oxidation on GEM was also limited. Thus, neither NO_2 nor O_3 exhibited considerable effects on regulating the GEM variation.

To more explicitly identify the drivers to the dynamic variation in GEM, a process analysis of GEM pollution episodes was conducted. One pollution episode was defined as having its average GEM concentration for more than 35 % of the day before the episode and lasting for more than 3 d. Based on this criterion, two pollution episodes (PE1 and PE2) before the lockdown, one pollution episode (PE3) during the lockdown, and one pollution episode (PE4) after the lockdown were selected (Fig. S6). As shown in Fig. 5, the drivers of the first two pollution episodes were significantly different from

the last two. The main influencing factors in PE1 were $PM_{2.5}$ and CO, which represented anthropogenic sources, contributing 0.65 and $0.51 \, \mathrm{ng \, m^{-3}}$ to the GEM variation, respectively. Similar to PE1, $PM_{2.5}$ and CO in PE2 contributed the most to the GEM variation in 0.35 and $0.12 \, \mathrm{ng \, m^{-3}}$, respectively. This indicated that the two mercury pollution episodes before the lockdown were mainly driven by anthropogenic sources. In contrast, in PE3 and PE4, temperature ranked the first among all the variables, with a contribution to GEM of 0.10 and $0.14 \, \mathrm{ng \, m^{-3}}$, respectively. This suggested that these two pollution episodes during and after the lockdown occurred under the dominance of natural sources.

In addition, we found that there was a tradeoff between the SHAP value of temperature and the SHAP value of $PM_{2.5}$ and CO. As shown in Fig. 5b–c, the SHAP value of temperature decreased with the increase in the SHAP value of $PM_{2.5}$ and CO throughout the study period. This probably suggests that the increase in anthropogenic GEM emissions may inhibit the release of natural sources to some extent, which will be discussed later.

## 3.4 Response of natural release of GEM to the lockdown

To quantify the changes in the contribution of different sources to GEM, we applied the PMF model to analyze the sources of GEM during the whole study period. Figure S7 shows the resolved factors and factor loadings, which were similar to the results by previous study at the same site (Qin et al., 2020). A total of six sources were resolved, namely coal combustion, with high loadings of SO_4^{2-}, Pb, K^+, As, and Se, natural surface emissions, with high loadings of temperature and NH_3, vehicle emissions, with high loadings of NO, ship emissions, with high loading of Ni, iron and steel production, with high loadings of Fe, Cr, and Mn, and cement production, with high loading of Ca. The mean contributions of the six factors above to GEM were 55 %, 28 %, 7 %, 5 %, 3 %, and 3 %, respectively (Fig. S7). To evaluate the uncertainty in the PMF results, the Fpeak model run at the strength of 0.5, −0.5, 1, and −1 were conducted by using the rotation tools in PMF. The changes in Q value (dQ) due to the Fpeak rotation were less than 1 % of the base run Q (robust) value (Table S3), which is less than the benchmark value of 5 %. The profiles and contributions of each source were also examined, and there were no significant differences between the factor contributions of the base run and rotation results, especially for coal combustion and natural surface emissions. Hence, the base run results were used in this study.

Figure 6a shows the time series of apportioned GEM concentrations and relative contributions from six sources during three periods. Significant changes in the sources of GEM were observed due to the lockdown. The contribution of coal combustion fell from 60 % before the lockdown to 51 % during the lockdown and 48 % after the lockdown. On the contrary, the relative contribution of natural surface emissions
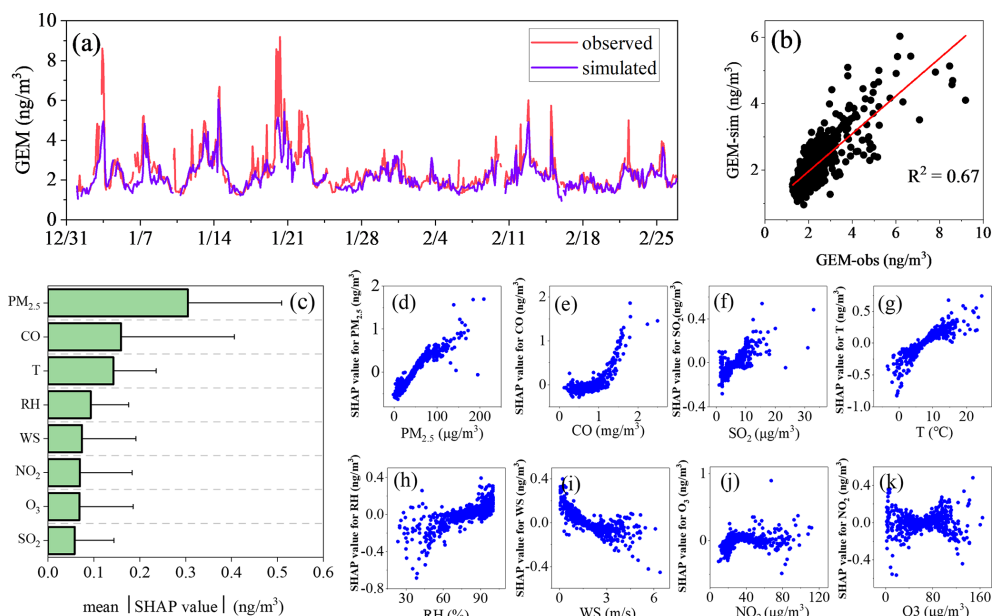
Figure 4. (a) Time series of ANN simulated and observed GEM concentrations during the study period. **(b)** Linear correlation between observed and ANN simulated GEM concentrations. **(c)** The ranking of input features calculated via the SHAP algorithm. **(d–k)** Relationship between the SHAP value and the corresponding concentration of each feature.
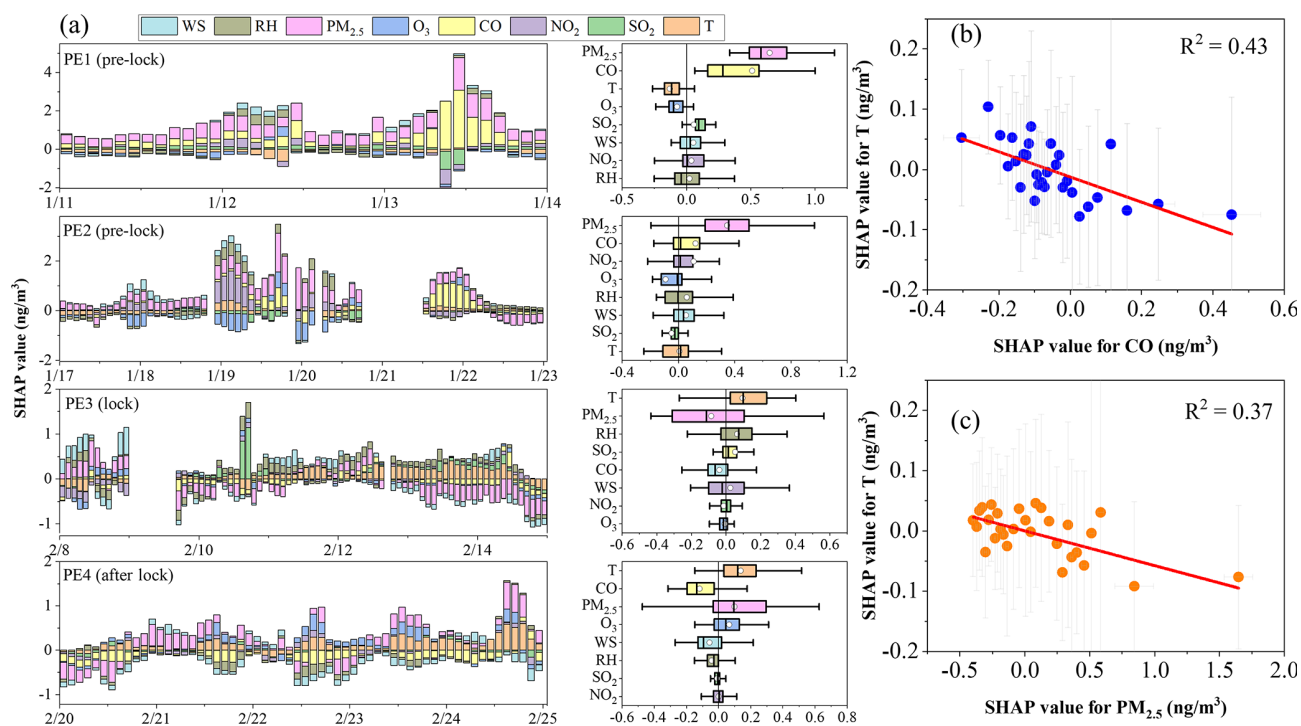
Figure 5. (a) Time series and box plots of each feature's SHAP value during the four mercury pollution episodes. **(b–c)** Relationship between the SHAP value of temperature and SHAP value of CO and PM$_{2.5}$ during the whole study period.
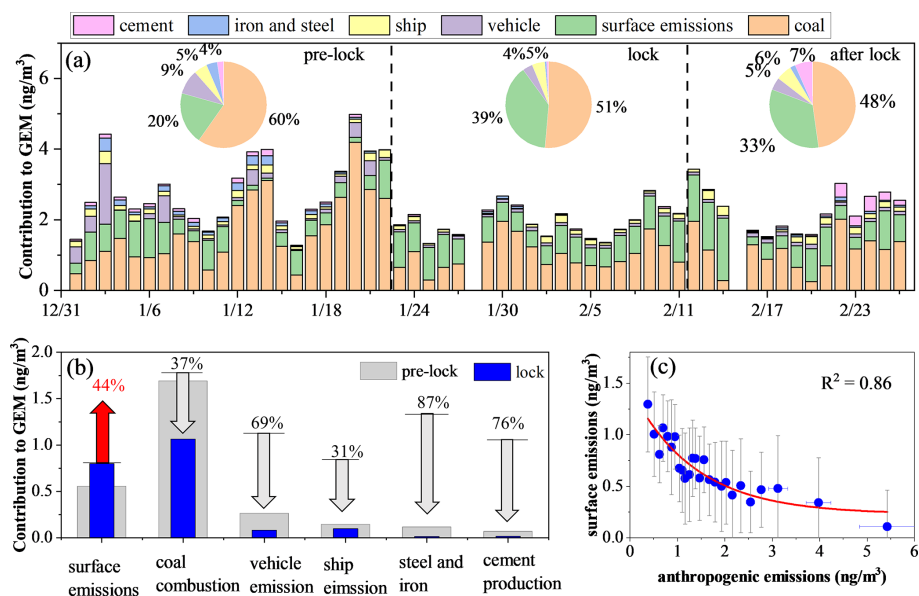
Figure 6. (a) Daily average concentrations of apportioned GEM from six sources based on PMF modeling. Pie charts represent the relative contribution of the six sources to GEM during three periods. **(b)** Changes in the absolute contribution of natural and anthropogenic sources to GEM before and during the lockdown. **(c)** Relationship between absolute contribution of natural surface emissions and anthropogenic sources to GEM during the whole study period.

rose significantly from 20 % before the lockdown to 39 % during the lockdown, and then dropped slightly to 33 % after the lockdown. In addition to the increased relative contribution of natural surface emissions, its absolute contribution to the GEM concentration increased significantly from $0.55\,\mathrm{ng\,m^{-3}}$ before the lockdown to $0.80\,\mathrm{ng\,m^{-3}}$ during the lockdown, i.e., a 44 % increase (Fig. 6b). Considering that the synoptic conditions varied little before and during the lockdown, both increases in the absolute and relative contribution of natural surface emissions to GEM during the lockdown should be stimulated by the significant reduction in anthropogenic mercury emissions. Indeed, Fig. 6c shows that the absolute contribution of natural surface emissions to GEM and the contribution of anthropogenic sources exhibited a significant negative correlation throughout the study period ($R^2 = 0.86$). This indicated that the significant reduction in the anthropogenic emissions would lead to a significant decrease in the GEM concentration, thereby disrupting the exchange balance of mercury between the natural surfaces (including soil, vegetation, and waterbodies, etc.) and the atmosphere, resulting in an increase in natural surface release to compensate for the decrease in GEM concentration in the atmosphere.

4   Conclusions and implications

In this work, we investigated the changes in the impact of anthropogenic and natural sources on GEM in the suburbs of eastern China in early 2020. Due to the COVID-19 lockdown, GEM was significantly reduced by $0.72\,\mathrm{ng\,m^{-3}}$ com-

pared to that before the lockdown. However, the reduction extent of GEM was not as strong as most of the other gaseous pollutants (NO_2 and CO) and primary aerosol species (EC, BC, Pb, and As). Before the lockdown, when anthropogenic emissions dominated, GEM showed no correlation with temperature and negative correlations with wind speed and the height of PBL. In contrast, GEM showed a significant correlation with temperature, while the relationship between GEM and wind speed/PBL disappeared during the lockdown, suggesting the enhanced natural emissions of mercury. By applying a machine learning model, GEM was well simulated, and the results were interpreted by the SHapley Additive exPlanations approach. It was found that the mercury pollution episodes before the lockdown were driven by anthropogenic sources, while they were mainly driven by natural sources during and after the lockdown. Source apportionment results showed that the relative contribution of natural sources to GEM during the lockdown reached 39 %, which was significantly higher than that before the lockdown (20 %). The absolute contribution of natural sources to GEM during the lockdown was about $0.80\,\mathrm{ng\,m^{-3}}$, which was 44 % higher than that before the lockdown. Finally, we revealed the negative correlation between the absolute contribution of natural sources and anthropogenic sources, suggesting the natural release of mercury could be enhanced in response to the significant reduction in anthropogenic mercury emissions.

In the long-term, the surface ambient mercury concentration in the Northern Hemisphere decreased by 30 %–40 % from 1990 to 2010 (Slemr et al., 2011; Soerensen et al., 2012; Cole et al., 2014). From 2013 to 2017, the gaseous total mer-

cury concentration in China decreased by about 12 % (Liu et al., 2019). It has been long recognized that the mitigation of anthropogenic mercury emissions regulated this global or regional trend, while the role of natural mercury emissions is less known. Specifically, the response of natural mercury release to the reduction in ambient Hg^0 concentration is ambiguous, which limits a better understanding of the role of natural sources in global mercury cycling. In this study, the COVID-19 lockdown provided a natural experiment for assessing the dynamic behavior of natural and anthropogenic contributions to gaseous elementary mercury by different means. As shown in Fig. S8, the sum of the SHAP values of CO and $PM_{2.5}$ exhibited a good positive correlation, with the concentration of GEM contributed by anthropogenic sources based on PMF modeling ($R^2 = 0.72$). Moderate correlation was also derived between the SHAP value of temperature and the concentration of GEM contributed by natural sources ($R^2 = 0.50$). This indicated that the results of the machine learning with an explainable approach and the traditional receptor model were consistent and also corroborated each other. This study highlighted that machine learning coupled with reliable interpretation methods can well quantify the role of different factors in the process of air pollution, showing great potential in the fields of atmospheric science. However, we realize that the performance of machine learning in simulating atmospheric mercury in this study has yet to be improved. Continuous long-term observations of atmospheric mercury with more monitoring sites are desired to ensure a more adequate training data set. Also, more relevant environment parameters for GEM are needed to further improve the training performance of the machine learning model. In addition, different machine learning methods such as artificial neural network, decision tree, random forest, and Bayesian learning should be evaluated to choose an optimal solution.

The natural release of mercury mainly comes from the exchange between the natural surfaces and the atmosphere, including the following two processes: (1) the formation of volatile Hg^0 in the surface and (2) the mass transfer of Hg^0 between the interfaces (Zhu et al., 2016). At locations with high ambient Hg^0 concentrations (e.g., mining areas and landfills), the exchange of mercury between the surface and the atmosphere is always dominated by deposition, regardless of changes in meteorological conditions (Bash and Miller, 2007; Wang et al., 2007; Zhu et al., 2013). Fluctuations in ambient Hg^0 concentrations can change the Hg^0 concentration gradient at the interfaces and thus affect the Hg^0 exchange flux (Xin and Gustin, 2007). The results of this study imply that the decline in global anthropogenic mercury emissions could stimulate increases in natural surface releases, which may pose challenges to future control of atmospheric mercury pollution.

Author contributions. XQ, CD, and KH designed this study. XQ and SZ performed the measurements and data analysis. XW, QF, JC, YL, YD, and JH performed the data collection. XQ and KH wrote the paper. All co-authors have commented on and reviewed the paper.

References

Aas, K., Jullum, M., and Loland, A.: Explaining individual predictions when features are dependent: More accurate approximations to Shapley values, Artificial Intelligence, 298, 103502, https://doi.org/10.1016/j.artint.2021.103502, 2021.

Bahlmann, E., Ebinghaus, R., and Ruck, W.: Development and application of a laboratory flux measurement system (LFMS) for the investigation of the kinetics of mercury emissions from soils, J. Environ. Manag., 81, 114–125, https://doi.org/10.1016/j.jenvman.2005.09.022, 2006.

Bash, J. O. and Miller, D. R.: A note on elevated total gaseous mercury concentrations downwind from an agriculture field during tilling, Sci. Total Environ., 388, 379–388, https://doi.org/10.1016/j.scitotenv.2007.07.012, 2007.

Belis, C. A., Karagulian, F., Larsen, B. R., and Hopke, P. K.: Critical review and meta-analysis of ambient

particulate matter source apportionment using receptor models in Europe, Atmos. Environ., 69, 94–108, https://doi.org/10.1016/j.atmosenv.2012.11.009, 2013.

Carpi, A. and Lindberg, S. E.: Sunlight-mediated emission of elemental mercury from soil amended with municipal sewage sludge, Environ. Sci. Technol., 31, 2085–2091, https://doi.org/10.1021/es960910+, 1997.

Carpi, A., Fostier, A. H., Orta, O. R., dos Santos, J. C., and Gittings, M.: Gaseous mercury emissions from soil following forest loss and land use changes: Field experiments in the United States and Brazil, Atmos. Environ., 96, 423–429, https://doi.org/10.1016/j.atmosenv.2014.08.004, 2014.

Chang, Y., Huang, K., Xie, M., Deng, C., Zou, Z., Liu, S., and Zhang, Y.: First long-term and near real-time measurement of trace elements in China's urban atmosphere: temporal variability, source apportionment and precipitation effect, Atmos. Chem. Phys., 18, 11793–11812, https://doi.org/10.5194/acp-18-11793-2018, 2018.

Chang, Y., Huang, R. J., Ge, X., Huang, X., Hu, J., Duan, Y., Zou, Z., Liu, X., and Lehmann, M. F.: Puzzling haze events in China during the coronavirus (COVID-19) shutdown, Geophys. Res. Lett., 47, e2020GL088533, https://doi.org/10.1029/2020GL088533, 2020.

Cheng, I., Xu, X., and Zhang, L.: Overview of receptor-based source apportionment studies for speciated atmospheric mercury, Atmos. Chem. Phys., 15, 7877–7895, https://doi.org/10.5194/acp-15-7877-2015, 2015.

Chong, X., Wang, Y., Liu, R., Zhang, Y., Zhang, Y., and Zheng, W.: Pollution characteristics and source difference of gaseous elemental mercury between haze and non-haze days in winter, Sci. Total Environ., 678, 671–680, https://doi.org/10.1016/j.scitotenv.2019.04.338, 2019.

Cole, A. S., Steffen, A., Eckley, C. S., Narayan, J., Pilote, M., Tordon, R., Graydon, J. A., St Louis, V. L., Xu, X., and Branfireun, B. A.: A Survey of Mercury in Air and Precipitation across Canada: Patterns and Trends, Atmosphere, 5, 635–668, https://doi.org/10.3390/atmos5030635, 2014.

Custodio, D., Ebinghaus, R., Spain, T. G., and Bieser, J.: Source apportionment of atmospheric mercury in the remote marine atmosphere: Mace Head GAW station, Irish western coast, Atmos. Chem. Phys., 20, 7929–7939, https://doi.org/10.5194/acp-20-7929-2020, 2020.

Driscoll, C. T., Mason, R. P., Chan, H. M., Jacob, D. J., and Pirrone, N.: Mercury as a global pollutant: sources, pathways, and effects, Environ. Sci. Technol., 47, 4967–4983, https://doi.org/10.1021/es305071v, 2013.

Fu, X. W., Zhang, H., Lin, C.-J., Feng, X. B., Zhou, L. X., and Fang, S. X.: Correlation slopes of GEM / CO, GEM / CO$_2$, and GEM / CH$_4$ and estimated mercury emissions in China, South Asia, the Indochinese Peninsula, and Central Asia derived from observations in northwestern and southwestern China, Atmos. Chem. Phys., 15, 1013–1028, https://doi.org/10.5194/acp-15-1013-2015, 2015.

Giang, A. and Selin, N. E.: Benefits of mercury controls for the United States, P. Natl. Acad. Sci. USA, 113, 286–291, https://doi.org/10.1073/pnas.1514395113, 2016.

Gibson, M. D., Haelssig, J., Pierce, J. R., Parrington, M., Franklin, J. E., Hopper, J. T., Li, Z., and Ward, T. J.: A comparison of four receptor models used to quantify the boreal wildfire smoke

contribution to surface PM$_{2.5}$ in Halifax, Nova Scotia during the BORTAS-B experiment, Atmos. Chem. Phys., 15, 815–827, https://doi.org/10.5194/acp-15-815-2015, 2015.

Grange, S. K., Carslaw, D. C., Lewis, A. C., Boleti, E., and Hueglin, C.: Random forest meteorological normalisation models for Swiss PM$_{10}$ trend analysis, Atmos. Chem. Phys., 18, 6223–6239, https://doi.org/10.5194/acp-18-6223-2018, 2018.

Gustin, M. S., Engle, M., Ericksen, J., Xin, M., Krabbenhoft, D., Lindberg, S., Olund, S., and Rytuba, J.: New insights into mercury exchange between air and substrate, Geochim. Cosmochim. Acta, 69, A700–A700, 2005.

Holmes, C. D., Jacob, D. J., Corbitt, E. S., Mao, J., Yang, X., Talbot, R., and Slemr, F.: Global atmospheric model for mercury including oxidation by bromine atoms, Atmos. Chem. Phys., 10, 12037–12057, https://doi.org/10.5194/acp-10-12037-2010, 2010.

Hopke, P. K.: Review of receptor modeling methods for source apportionment, J. Air Waste Manage., 66, 237–259, https://doi.org/10.1080/10962247.2016.1140693, 2016.

Horowitz, H. M., Jacob, D. J., Zhang, Y., Dibble, T. S., Slemr, F., Amos, H. M., Schmidt, J. A., Corbitt, E. S., Marais, E. A., and Sunderland, E. M.: A new mechanism for atmospheric mercury redox chemistry: implications for the global mercury budget, Atmos. Chem. Phys., 17, 6353–6371, https://doi.org/10.5194/acp-17-6353-2017, 2017.

Hou, L., Dai, Q., Song, C., Liu, B., Guo, F., Dai, T., Li, L., Liu, B., Bi, X., Zhang, Y., and Feng, Y.: Revealing Drivers of Haze Pollution by Explainable Machine Learning, Environ. Sci. Tech. Let., 9, 112–119, https://doi.org/10.1021/acs.estlett.1c00865, 2022.

Huang, K.: Gaseous elementary mercury and other air pollutants data during COVID-19, Zenodo [data set], https://doi.org/10.5281/zenodo.6654670, 2022.

Huang, S. and Zhang, Y.: Interannual Variability of Air-Sea Exchange of Mercury in the Global Ocean: The "Seesaw Effect" in the Equatorial Pacific and Contributions to the Atmosphere, Environ. Sci. Technol., 55, 7145–7156, https://doi.org/10.1021/acs.est.1c00691, 2021.

Huang, X., Ding, A., Gao, J., Zheng, B., Zhou, D., Qi, X., Tang, R., Wang, J., Ren, C., Nie, W., Chi, X., Xu, Z., Chen, L., Li, Y., Che, F., Pang, N., Wang, H., Tong, D., Qin, W., Cheng, W., Liu, W., Fu, Q., Liu, B., Chai, F., Davis, S. J., Zhang, Q., and He, K.: Enhanced secondary pollution offset reduction of primary emissions during COVID-19 lockdown in China, Natl. Sci. Rev., 8, nwaa137, https://doi.org/10.1093/nsr/nwaa137, 2021.

Jiskra, M., Sonke, J. E., Obrist, D., Bieser, J., Ebinghaus, R., Myhre, C. L., Pfaffhuber, K. A., Wangberg, I., Kyllonen, K., Worthy, D., Martin, L. G., Labuschagne, C., Mkololo, T., Ramonet, M., Magand, O., and Dommergue, A.: A vegetation control on seasonal variations in global atmospheric mercury concentrations, Nat. Geosci., 11, 244–250, https://doi.org/10.1038/s41561-018-0078-8, 2018.

Kumar, I. E., Venkatasubramanian, S., Scheidegger, C., and Friedler, S. A.: Problems with Shapley-value-based explanations as feature importance measures, International Conference on Machine Learning (ICML), Electr. Network, https://arxiv.org/pdf/2002.11097.pdf (last access: 16 December 2022), 13–18 July 2020, Vienna, Austria, 2020.

Li, H., Huang, K., Fu, Q., Lin, Y., Chen, J., Deng, C., Tian, X., Tang, Q., Song, Q., and Wei, Z.: Airborne black carbon vari-

ations during the COVID-19 lockdown in the Yangtze River Delta megacities suggest actions to curb global warming, Environ. Chem. Lett., 20, 1–10, https://doi.org/10.1007/s10311-021-01327-3, 2021.

Lindberg, S., Bullock, R., Ebinghaus, R., Engstrom, D., Feng, X. B., Fitzgerald, W., Pirrone, N., Prestbo, E., and Seigneur, C.: A synthesis of progress and uncertainties in attributing the sources of mercury in deposition, Ambio, 36, 19–32, 2007.

Liu, K., Wang, S., Wu, Q., Wang, L., Ma, Q., Zhang, L., Li, G., Tian, H., Duan, L., and Hao, J.: A Highly Resolved Mercury Emission Inventory of Chinese Coal-Fired Power Plants, Environ. Sci. Technol., 52, 2400–2408, https://doi.org/10.1021/acs.est.7b06209, 2018.

Liu, K., Wu, Q., Wang, L., Wang, S., Liu, T., Ding, D., Tang, Y., Li, G., Tian, H., Duan, L., Wang, X., Fu, X., Feng, X., and Hao, J.: Measure-Specific Effectiveness of Air Pollution Control on China's Atmospheric Mercury Concentration and Deposition during 2013–2017, Environ. Sci. Technol., 53, 8938–8946, https://doi.org/10.1021/acs.est.9b02428, 2019.

Lundberg, S. M. and Lee, S.-I.: A Unified Approach to Interpreting Model Predictions, 31st Annual Conference on Neural Information Processing Systems (NIPS), 4–9 December 2017, Long Beach, CA, USA, 2017.

Lundberg, S. M., Nair, B., Vavilala, M. S., Horibe, M., Eisses, M. J., Adams, T., Liston, D. E., Low, D. K.-W., Newman, S.-F., Kim, J., and Lee, S.-I.: Explainable machine-learning predictions for the prevention of hypoxaemia during surgery, Nature Biomedical Engineering, 2, 749–760, https://doi.org/10.1038/s41551-018-0304-0, 2018.

Lundberg, S. M., Erion, G., Chen, H., DeGrave, A., Prutkin, J. M., Nair, B., Katz, R., Himmelfarb, J., Bansal, N., and Lee, S. I.: From Local Explanations to Global Understanding with Explainable AI for Trees, Nat. Mach. Intell., 2, 56–67, https://doi.org/10.1038/s42256-019-0138-9, 2020.

Mangalathu, S., Hwang, S.-H., and Jeon, J.-S.: Failure mode and effects analysis of RC members based on machine-learning-based SHapley Additive exPlanations (SHAP) approach, Eng. Struct., 219, 110927, https://doi.org/10.1016/j.engstruct.2020.110927, 2020.

Mao, H., Cheng, I., and Zhang, L.: Current understanding of the driving mechanisms for spatiotemporal variations of atmospheric speciated mercury: a review, Atmos. Chem. Phys., 16, 12897–12924, https://doi.org/10.5194/acp-16-12897-2016, 2016.

Mazur, M., Mitchell, C. P. J., Eckley, C. S., Eggert, S. L., Kolka, R. K., Sebestyen, S. D., and Swain, E. B.: Gaseous mercury fluxes from forest soils in response to forest harvesting intensity: A field manipulation experiment, Sci. Total Environ., 496, 678–687, https://doi.org/10.1016/j.scitotenv.2014.06.058, 2014.

Moore, C. and Carpi, A.: Mechanisms of the emission of mercury from soil: Role of UV radiation, J. Geophys. Res.-Atmos., 110, D24302, https://doi.org/10.1029/2004jd005567, 2005.

Obrist, D., Kirk, J. L., Zhang, L., Sunderland, E. M., Jiskra, M., and Selin, N. E.: A review of global environmental mercury processes in response to human and natural perturbations: Changes of emissions, climate, and land use, Ambio, 47, 116–140, https://doi.org/10.1007/s13280-017-1004-9, 2018.

Outridge, P. M., Mason, R. P., Wang, F., Guerrero, S., and Heimbürger-Boavida, L. E.: Updated Global and Oceanic Mercury Budgets for the United Nations Global Mercury As-

sessment 2018, Environ. Sci. Technol., 52, 11466–11477, https://doi.org/10.1021/acs.est.8b01246, 2018.

Pannu, R., Siciliano, S. D., and O'Driscoll, N. J.: Quantifying the effects of soil temperature, moisture and sterilization on elemental mercury formation in boreal soils, Environ. Pollut., 193, 138–146, https://doi.org/10.1016/j.envpol.2014.06.023, 2014.

Pirrone, N., Cinnirella, S., Feng, X., Finkelman, R. B., Friedli, H. R., Leaner, J., Mason, R., Mukherjee, A. B., Stracher, G. B., Streets, D. G., and Telmer, K.: Global mercury emissions to the atmosphere from anthropogenic and natural sources, Atmos. Chem. Phys., 10, 5951–5964, https://doi.org/10.5194/acp-10-5951-2010, 2010.

Poissant, L., Pilote, M., Constant, P., Beauvais, C., Zhang, H. H., and Xu, X. H.: Mercury gas exchanges over selected bare soil and flooded sites in the bay St. Francois wetlands (Quebec, Canada), Atmos. Environ., 38, 4205–4214, https://doi.org/10.1016/j.atmosenv.2004.03.068, 2004.

Qi, Y., Li, Q., Karimian, H., and Liu, D.: A hybrid model for spatiotemporal forecasting of PM2.5 based on graph convolutional neural network and long short-term memory, Sci. Total Environ., 664, 1–10, https://doi.org/10.1016/j.scitotenv.2019.01.333, 2019.

Qin, X., Wang, X., Shi, Y., Yu, G., Zhao, N., Lin, Y., Fu, Q., Wang, D., Xie, Z., Deng, C., and Huang, K.: Characteristics of atmospheric mercury in a suburban area of east China: sources, formation mechanisms, and regional transport, Atmos. Chem. Phys., 19, 5923–5940, https://doi.org/10.5194/acp-19-5923-2019, 2019.

Qin, X., Zhang, L., Wang, G., Wang, X., Fu, Q., Xu, J., Li, H., Chen, J., Zhao, Q., Lin, Y., Huo, J., Wang, F., Huang, K., and Deng, C.: Assessing contributions of natural surface and anthropogenic emissions to atmospheric mercury in a fast-developing region of eastern China from 2015 to 2018, Atmos. Chem. Phys., 20, 10985–10996, https://doi.org/10.5194/acp-20-10985-2020, 2020.

Qin, X., Zhou, S., Li, H., Wang, G., Wang, X., Fu, Q., Duan, Y., Lin, Y., Huo, J., Huang, K., and Deng, C.: Simulation of Spatiotemporal Trends of Gaseous Elemental Mercury in the Yangtze River Delta of Eastern China by an Artificial Neural Network, Environ. Sci. Tech. Lett., 9, 205–211, https://doi.org/10.1021/acs.estlett.1c01025, 2022.

Selin, N. E., Jacob, D. J., Park, R. J., Yantosca, R. M., Strode, S., Jaegle, L., and Jaffe, D.: Chemical cycling and deposition of atmospheric mercury: Global constraints from observations, J. Geophys. Res.-Atmos., 112, D02308, https://doi.org/10.1029/2006jd007450, 2007.

Slemr, F., Brunke, E.-G., Ebinghaus, R., and Kuss, J.: Worldwide trend of atmospheric mercury since 1995, Atmos. Chem. Phys., 11, 4779–4787, https://doi.org/10.5194/acp-11-4779-2011, 2011.

Soerensen, A. L., Jacob, D. J., Streets, D. G., Witt, M. L. I., Ebinghaus, R., Mason, R. P., Andersson, M., and Sunderland, E. M.: Multi-decadal decline of mercury in the North Atlantic atmosphere explained by changing subsurface seawater concentrations, Geophys. Res. Lett., 39, L21810, https://doi.org/10.1029/2012gl053736, 2012.

Steenhuisen, F. and Wilson, S. J.: Development and application of an updated geospatial distribution model for gridding

2015 global mercury emissions, Atmos. Environ., 211, 138–150, https://doi.org/10.1016/j.atmosenv.2019.05.003, 2019.

Stirnberg, R., Cermak, J., Kotthaus, S., Haeffelin, M., Andersen, H., Fuchs, J., Kim, M., Petit, J.-E., and Favez, O.: Meteorology-driven variability of air pollution (PM$_1$) revealed with explainable machine learning, Atmos. Chem. Phys., 21, 3919–3948, https://doi.org/10.5194/acp-21-3919-2021, 2021.

Streets, D. G., Devane, M. K., Lu, Z. F., Bond, T. C., Sunderland, E. M., and Jacob, D. J.: All-Time Releases of Mercury to the Atmosphere from Human Activities, Environ. Sci. Technol., 45, 10485–10491, https://doi.org/10.1021/es202765m, 2011.

Streets, D. G., Horowitz, H. M., Lu, Z., Levin, L., Thackray, C. P., and Sunderland, E. M.: Global and regional trends in mercury emissions and concentrations, 2010–2015, Atmos. Environ., 201, 417–427, https://doi.org/10.1016/j.atmosenv.2018.12.031, 2019.

Sun, Y., Chen, C., Zhang, Y., Xu, W., Zhou, L., Cheng, X., Zheng, H., Ji, D., Li, J., Tang, X., Fu, P., and Wang, Z.: Rapid formation and evolution of an extreme haze episode in Northern China during winter 2015, Scientific Reports, 6, 27151, https://doi.org/10.1038/srep27151, 2016.

Tang, Y., Wang, S., Wu, Q., Liu, K., Wang, L., Li, S., Gao, W., Zhang, L., Zheng, H., Li, Z., and Hao, J.: Recent decrease trend of atmospheric mercury concentrations in East China: the influence of anthropogenic emissions, Atmos. Chem. Phys., 18, 8279–8291, https://doi.org/10.5194/acp-18-8279-2018, 2018.

Vu, T. V., Shi, Z., Cheng, J., Zhang, Q., He, K., Wang, S., and Harrison, R. M.: Assessing the impact of clean air action on air quality trends in Beijing using a machine learning technique, Atmos. Chem. Phys., 19, 11303–11314, https://doi.org/10.5194/acp-19-11303-2019, 2019.

Wang, C., Feng, L., and Qi, Y.: Explainable deep learning predictions for illness risk of mental disorders in Nanjing, China, Environ. Res., 202, 111740, https://doi.org/10.1016/j.envres.2021.111740, 2021.

Wang, G. C., Huang, K., Fu, Q. Y., Chen, J., Huo, J. T., Zhao, Q. B., Duan, Y. S., Lin, Y. F., Yang, F., Zhang, W. J., Li, H., Xu, J., Qin, X. F., Zhao, N., and Deng, C. R.: Response of PM$_{2.5}$-bound elemental species to emission variations and associated health risk assessment during the COVID-19 pandemic in a coastal megacity, J. Environ. Sci., 122, 115–127, https://doi.org/10.1016/j.jes.2021.10.005, 2022a.

Wang, G. C., Chen, J., Xu, J., Yun, L., Zhang, M. D., Li, H., Qin, X. F., Deng, C. R., Zheng, H. T., Gui, H. Q., Liu, J. G., and Huang, K.: Atmospheric Processing at the Sea-Land Interface Over the South China Sea: Secondary Aerosol Formation, Aerosol Acidity, and Role of Sea Salts, J. Geophys. Res.-Atmos., 127, e2021JD036255, https://doi.org/10.1029/2021jd036255, 2022b.

Wang, S. F., Feng, X. B., Qiu, G. L., Fu, X. W., and Wei, Z. Q.: Characteristics of mercury exchange flux between soil and air in the heavily air-polluted area, eastern Guizhou, China, Atmos. Environ., 41, 5584–5594, https://doi.org/10.1016/j.atmosenv.2007.03.002, 2007.

Wang, X., Lin, C.-J., and Feng, X.: Sensitivity analysis of an updated bidirectional air–surface exchange model for elemental mercury vapor, Atmos. Chem. Phys., 14, 6273–6287, https://doi.org/10.5194/acp-14-6273-2014, 2014.

Wang, X., Lin, C.-J., Yuan, W., Sommar, J., Zhu, W., and Feng, X.: Emission-dominated gas exchange of elemental mercury vapor

over natural surfaces in China, Atmos. Chem. Phys., 16, 11125–11143, https://doi.org/10.5194/acp-16-11125-2016, 2016.

Wanninkhof, R.: Relationship between wind speed and gas exchange over the ocean revisited, Limnol. Oceanogr.-Meth., 12, 351–362, https://doi.org/10.4319/lom.2014.12.351, 2014.

Wen, M., Wu, Q., Li, G., Wang, S., Li, Z., Tang, Y., Xu, L., and Liu, T.: Impact of ultra-low emission technology retrofit on the mercury emissions and cross-media transfer in coal-fired power plants, J. Hazard. Mater., 396, 122729, https://doi.org/10.1016/j.jhazmat.2020.122729, 2020.

Wu, Q., Tang, Y., Wang, L., Wang, S., Han, D., Ouyang, D., Jiang, Y., Xu, P., Xue, Z., and Hu, J.: Impact of emission reductions and meteorology changes on atmospheric mercury concentrations during the COVID-19 lockdown, Sci. Total Environ., 750, 142323, https://doi.org/10.1016/j.scitotenv.2020.142323, 2021.

Wu, Q. R., Wang, S. X., Li, G. L., Liang, S., Lin, C. J., Wang, Y. F., Cai, S. Y., Liu, K. Y., and Hao, J. M.: Temporal Trend and Spatial Distribution of Speciated Atmospheric Mercury Emissions in China During 1978–2014, Environ. Sci. Technol., 50, 13428–13435, https://doi.org/10.1021/acs.est.6b04308, 2016.

Wu, Q. R., Wang, S. X., Liu, K. Y., Li, G. L., and Hao, J. M.: Emission-Limit-Oriented Strategy To Control Atmospheric Mercury Emissions in Coal-Fired Power Plants toward the Implementation of the Minamata Convention, Environ. Sci. Technol., 52, 11087–11093, https://doi.org/10.1021/acs.est.8b02250, 2018.

Xin, M. and Gustin, M. S.: Gaseous elemental mercury exchange with low mercury containing soils: Investigation of controlling factors, Appl. Geochem., 22, 1451–1466, https://doi.org/10.1016/j.apgeochem.2007.02.006, 2007.

Xu, J., Wang, Q. Z., Deng, C. R., McNeill, V. F., Fankhauser, A., Wang, F. W., Zheng, X. J., Shen, J. D., Huang, K., and Zhuang, G. S.: Insights into the characteristics and sources of primary and secondary organic carbon: High time resolution observation in urban Shanghai, Environ. Pollut., 233, 1177–1187, https://doi.org/10.1016/j.envpol.2017.10.003, 2018.

Xu, J., Chen, J., Shi, Y. J., Zhao, N., Qin, X. F., Yu, G. Y., Liu, J. M., Lin, Y. F., Fu, Q. Y., Weber, R. J., Lee, S. H., Deng, C. R., and Huang, K.: First Continuous Measurement of Gaseous and Particulate Formic Acid in a Suburban Area of East China: Seasonality and Gas-Particle Partitioning, Acs Earth and Space Chemistry, 4, 157–167, https://doi.org/10.1021/acsearthspacechem.9b00210, 2020.

Xu, X., Liao, Y., Cheng, I., and Zhang, L.: Potential sources and processes affecting speciated atmospheric mercury at Kejimkujik National Park, Canada: comparison of receptor models and data treatment methods, Atmos. Chem. Phys., 17, 1381–1400, https://doi.org/10.5194/acp-17-1381-2017, 2017.

Yang, J., Wen, Y., Wang, Y., Zhang, S., Pinto, J. P., Pennington, E. A., Wang, Z., Wu, Y., Sander, S. P., Jiang, J. H., Hao, J., Yung, Y. L., and Seinfeld, J. H.: From COVID-19 to future electrification: Assessing traffic impacts on air quality by a machine-learning model, P. Natl. Acad. Sci. USA, 118, e2102705118, https://doi.org/10.1073/pnas.2102705118, 2021.

Yin, X., Kang, S., de Foy, B., Ma, Y., Tong, Y., Zhang, W., Wang, X., Zhang, G., and Zhang, Q.: Multi-year monitoring of atmospheric total gaseous mercury at a remote high-altitude site (Nam Co, 4730 m a.s.l.) in the inland Tibetan Plateau region, Atmos. Chem.

Phys., 18, 10557–10574, https://doi.org/10.5194/acp-18-10557-2018, 2018.

Yu, Y., He, S., Wu, X., Zhang, C., Yao, Y., Liao, H., Wang, Q., and Xie, M.: PM$_{2.5}$ elements at an urban site in Yangtze River Delta, China: High time-resolved measurement and the application in source apportionment, Environ. Pollut., 253, 1089–1099, https://doi.org/10.1016/j.envpol.2019.07.096, 2019.

Zhang, L., Wang, S. X., Wang, L., and Hao, J. M.: Atmospheric mercury concentration and chemical speciation at a rural site in Beijing, China: implications of mercury emission sources, Atmos. Chem. Phys., 13, 10505–10516, https://doi.org/10.5194/acp-13-10505-2013, 2013.

Zhang, L., Wang, S., Wu, Q., Wang, F., Lin, C.-J., Zhang, L., Hui, M., Yang, M., Su, H., and Hao, J.: Mercury transformation and speciation in flue gases from anthropogenic emission sources: a critical review, Atmos. Chem. Phys., 16, 2417–2433, https://doi.org/10.5194/acp-16-2417-2016, 2016a.

Zhang, Y., Jacob, D. J., Horowitz, H. M., Chen, L., Amos, H. M., Krabbenhoft, D. P., Slemr, F., St Louis, V. L., and Sunderland, E. M.: Observed decrease in atmospheric mercury explained by global decline in anthropogenic emissions, P. Natl. Acad. Sci. USA, 113, 526–531, https://doi.org/10.1073/pnas.1516312113, 2016b.

Zheng, B., Tong, D., Li, M., Liu, F., Hong, C., Geng, G., Li, H., Li, X., Peng, L., Qi, J., Yan, L., Zhang, Y., Zhao, H., Zheng, Y., He, K., and Zhang, Q.: Trends in China's anthropogenic emissions since 2010 as the consequence of clean air actions, Atmos. Chem. Phys., 18, 14095–14111, https://doi.org/10.5194/acp-18-14095-2018, 2018.

Zhong, S., Zhang, K., Wang, D., and Zhang, H.: Shedding light on "Black Box" machine learning models for predicting the reactivity of HO radicals toward organic compounds, Chem. Eng. J., 405, 126627, https://doi.org/10.1016/j.cej.2020.126627, 2021.

Zhu, J., Wang, T., Talbot, R., Mao, H., Hall, C. B., Yang, X., Fu, C., Zhuang, B., Li, S., Han, Y., and Huang, X.: Characteristics of atmospheric Total Gaseous Mercury (TGM) observed in urban Nanjing, China, Atmos. Chem. Phys., 12, 12103–12118, https://doi.org/10.5194/acp-12-12103-2012, 2012.

Zhu, W., Sommar, J., Li, Z., Feng, X., Lin, C.-J., and Li, G.: Highly elevated emission of mercury vapor due to the spontaneous combustion of refuse in a landfill, Atmos. Environ., 79, 540–545, https://doi.org/10.1016/j.atmosenv.2013.07.016, 2013.

Zhu, W., Lin, C.-J., Wang, X., Sommar, J., Fu, X., and Feng, X.: Global observations and modeling of atmosphere–surface exchange of elemental mercury: a critical review, Atmos. Chem. Phys., 16, 4451–4480, https://doi.org/10.5194/acp-16-4451-2016, 2016.